Estimation of Transonic Aircraft Aerodynamics to High Angles of Attack

John A. Axelson*
NASA Ames Research Center, Moffett Field, Calif.

A recently developed method for estimating transonic aircraft lift and induced drag to high angles of attack is described. Induced drag constitutes the major drag component at the higher angles; estimation of aircraft total drag coefficients requires the addition of suitable input minimum drag coefficients not evaluated in the present method. Following theoretical and empirical guidelines, explicit nonlinear equations are formulated for subsonic, transonic, and supersonic speeds; new algorithms are used for assessing compressibility effects and for analyzing transonic, shock-dominated flows that adhere to Laitone's limit Mach-number criterion. Viscous-dominated flows are not analyzed. The transonic influence of viscosity is accommodated indirectly by assigning designated inputs rather than extracted solutions for the chordwise locations of shock and separation. The method is extended to complete aircraft configurations by including accounts for nose lift, wing downwash field, and tail lift. Several comparisons of experiment and estimate are included.

Nomenclature

A	= aspect ratio
b	= span
C_D, c_d	= drag coefficient
C_L, c_ℓ	= lift coefficient
C_P	= pressure coefficient
c	= chord
$\bar{c}$	= wing mean aerodynamic chord
d	= $1.5-(M/4)\cos\bar{\Lambda}_{le}$ for $M \leq 1$
	= $1.5-(M^2/4)\cos\bar{\Lambda}_{le}$ for $1<M$
F	= compressibility factor
ℓ_t	= tail length from $\bar{c}/4$
M	= stream Mach number
P_{T_1}	= stream total pressure
p_2	= local static pressure
TR	= taper ratio
r/c	= leading-edge radius-to-chord ratio
S	= area
t/c	= thickness-to-chord ratio
V	= stream velocity
v	= downwash velocity
x, y	= Cartesian coordinates
y_0	= tail height from extended wing plane
α	= angle of attack
γ	= ratio of specific heats for air
ϵ	= downwash angle
Λ	= sweep angle

Subscripts

d	= detached shock
e	= leading-edge Mach limit condition
i	= induced
ℓ	= lower surface
loc	= local
le	= leading edge
lim	= limit value
m	= at maximum lift
sep	= separation
T	= trailing edge
u	= upper surface
w	= wake
x	= x component
2	= downstream of shock

Superscript

$(\bar{\ })$	= effective value, taking into account variation with angle of attack; e.g., $\bar{\Lambda} = \sin^{-1}(\sin\Lambda\cos\alpha)$

Presented as Paper 75-996 at the AIAA 1975 Aircraft Systems and Technology Meeting, Los Angeles, Calif., Aug. 4-7, 1975; submitted Sept. 9, 1975; revision received Jan. 24, 1977.
Index categories: Aerodynamics; Subsonic Flow; Transonic Flow.
*Aerospace Engineer. Member AIAA.

I. Introduction

THE transonic Mach number range encompasses the upper boundaries of most commercial jet-transport opearations and constitutes the primary arena for military aerial combat. No exact analytical method is available for estimating transonic aerodynamics to high angles of attack, but analytic methods are needed to estimate aircraft maneuvering performance. A method that has been used in several recent, computerized studies[1] of conceptual designs and optimizations is described here.

The unavailability of any rigorous method for calculating three-dimensional aerodynamic characteristics to high angles of attack was discussed by Smith in the 1974 AIAA Wright Brothers Lecture[2] and also in a more recent survey[3] of the application of computers to fluid dynamics. It is speculated in the latter that such a program might be available by the end of the decade. The pacing item cited in both of these reports is the current inability to account adequately for the influence of viscosity.

The present method is based on the premises that transonic flows past airfoils at high angles of attack are dominated by shock waves and that the local limiting Mach numbers and shock strengths are in conformance with Laitone's limit Mach-number criterion.[4] The primary role relegated to viscosity is its influence on the chordwise location of the shock wave and separation. These locations are not solved; rather they are incorporated as designated inputs and can be varied parametrically. The effects of varying the shock location are described in the correlations with experimental data. Pressure distributions and flow visualizations, when available, are useful aids in the choice of limit shock location.

New compressibility factors are introduced for the upper and lower surfaces of the wing. A nonlinear lift equation derived from the integration of downwash momentum is applied to three-dimensional, transonic flows containing limit shock waves and possibly related rotational flows. This equation is referred to as the nonpotential lift equation. The method is incorporated in the AEROX computer program, which is applicable to wings and to aircraft configurations.

The program accepts input values for the minimum drag coefficients and includes an option for estimating longitudinal trim drag. The effects of the propulsion system are not evaluated.

II. Approach

A. Flow Regimes

The formulations in the present method are organized according to the various flow regimes depicted in Fig. 1. Each regime is identified by a characteristic or dominant flow feature, and the boundaries between the zones are related to the most pertinent flow or geometric parameters.

Zone 1 encompasses the viscous stall region, where viscosity is considered the dominant flow feature. This regime and the delineation of its boundary are not covered in the present method. The compressible and shock-free regime, zone 2, adheres fairly closely to the traditional concept of compressible potential flow, except that new versions of compressibility factors are used here in order to cover large angles of attack and to be continuous through a Mach number of one. Zone 3 involves a new concept: the occurrence of the local limit Mach number at the leading edge. In this flow regime, the leading-edge thrust reaches a limiting value, and the additional lift is characterized as flat-plate nonpotential loading rather than potential lift. The onset of the leading-edge Mach-limited flow, zone 3, is estimated by the α_e equation derived later.

The surface Mach-limited flow regime, zone 4, involves the application of the Laitone limit Mach number along the upper surface to the designated shock location. The onset of zone 4 is specified when the lift estimated by the formulas for either zone 2 or 3 reaches the limit value specified for zone 4. This is the only zone in which shock location need be specified. Finally, the supersonic zone 5, lying to the right of the sonic leading-edge boundary ($M \cos\bar{\Lambda}_{\rm l.e.} = 1$), includes attached and detached bow shocks. Primary interest here is in the detached-shock case, which covers all conventional airfoils that have blunted leading edges.

B. Compressible (Shock-Free) Flow (Zone 2)

The aerodynamics for three-dimensional, compressible, shock-free flow are calculated from the equations developed below. The Prandtl aspect-ratio transformation and the cosine sweep ($c/4$) factor are applied to the incompressible, potential theory of Kutta-Joukowski [Eqs. (1-4)].

The two-dimensional incompressible relations are given by

$$c_\ell = 2\pi \sin\alpha \tag{1}$$

$$dc_\ell / d\alpha = 2\pi \cos\alpha \tag{2}$$

and the three-dimensional incompressible relations are given by

$$dC_L / d\alpha = 2\pi \cos\alpha \cos\bar{\Lambda} [A / A + 2] \tag{3}$$

$$C_L = 2\pi \sin\alpha \cos\bar{\Lambda} [A / (A+2)] \tag{4}$$

Compressible relations are obtained by applying separate compressibility factors to the lift components of the upper and lower surfaces of the airfoil [Eqs. (5-7)]

$$C_L = 2\pi \sin\alpha \cos\bar{\Lambda} [A / (A+2)] [(\bar{F}_u + \bar{F}_\ell)/2] \tag{5}$$

$$dC_L / d\alpha = \pi \cos\bar{\Lambda} [A / (A+2)] [\bar{F}_u \cos\alpha + (d\bar{F}_u / d\alpha) \sin\alpha + \bar{F}_\ell \cos\alpha] \tag{6}$$

$$C_{D_i} = C_L{}^2 / \pi A \tag{7}$$

where the compressible factors $\bar{F} = f(M, \Lambda, \alpha)$.

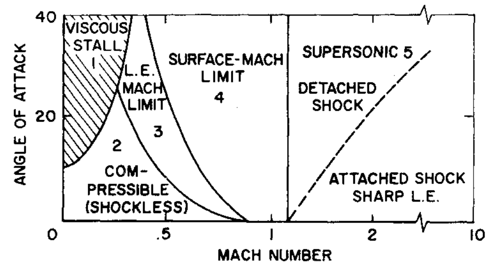

Fig. 1 Flow regimes.

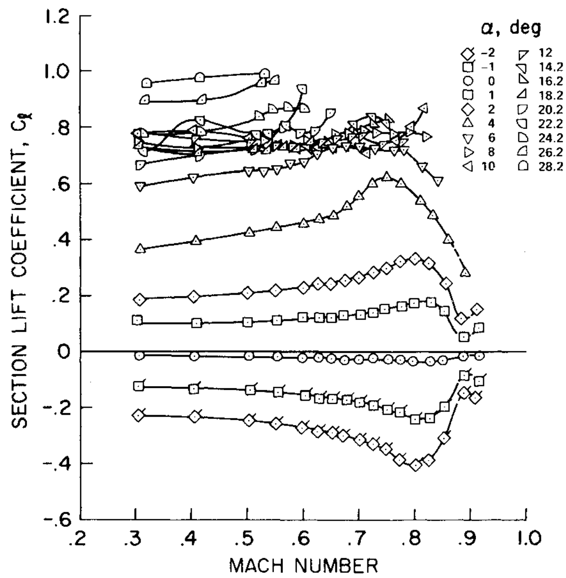

Fig. 2 Variation of section lift coefficient with Mach number for the NACA 64A010 airfoil at constant angles of attack.[6]

The compressibility factor $\bar{F}_u$ for the upper-surface lift is a form of the Prandtl-Glauert factor modified through a parabolic attenuation to a value of unity at maximum lift (set at $\alpha_m = 40°$)

$$\bar{F}_u = \frac{1 - (1 - \sqrt{1 - M^2 \cos^2\bar{\Lambda}})(\alpha/\alpha_m)^2}{\sqrt{1 - M^2 \cos^2\bar{\Lambda}}} \tag{8}$$

The rationale behind the attenuation in Eq. (8) is that the unaltered Prandtl-Glauert factor is derivable from the linearized perturbation potential, as demonstrated in Ref. 5, and would not be expected to apply at large angles of attack. Experimental evidence confirming the need for attenuation is shown in Fig. 2,[6] where a general flattening of the curves occurs for high angles of attack. The factor $\bar{F}_u$ is used only in zone 2 ($M < 0.9$).

The compressibility factor $\bar{F}_\ell$ for the lower surface lift is used in zones 2, 3, and 4 and involves a pitot compressibility factor modified for the effects of leading-edge sweep and angle of attack

$$\bar{F}_\ell = \frac{2}{\gamma M^2 \cos^2\bar{\Lambda}_{\rm l.e.}} \left\{ \left[1 + \left(\frac{\gamma - 1}{2} \right) M^2 \cos^2\bar{\Lambda}_{\rm l.e.} \right]^{\gamma/(\gamma-1)} - 1 \right\} \tag{9}$$

The factor given by Eq. (9) is the ratio of the leading-edge stagnation pressure in compressible flow to that in incompressible flow. The use of a separate compressibility factor for the lower surface lift was investigated long ago by Chaplygin.[7]

C. Leading-Edge Mach-Limited Flow (Zone 3)

The present method uses analytical flow models for the two transonic flows in which the limiting Mach number is reached at the leading edge or on the airfoil upper surface. Examples of both flows are typified by the pressure distributions of Fig. 3.[6] The pressure coefficients for the upper surface exhibit the leading-edge peaks for the lower Mach numbers and assume the flattened loading forward at the higher Mach numbers. The limit pressure coefficients (listed by the symbols) are approached closely at all but the lowest Mach number, where an angle of attack higher than 6.2° would be required. Note the negative pressure coefficients extending to the trailing edge at the two higher Mach numbers, an indication of separation over the aft portion of the airfoil for flow identified here as zone 4.

A summary of the minimum pressure coefficients from a large number of tests,[6,8-10] including two- and three-dimensional flows, is presented in Fig. 4. The points are identified according to the location of measurements, i.e., in the curvilinear flow around the leading edge, or in the essentially rectilinear flow along the airfoil surface. The surface values are in excellent agreement with the limit pressure coefficients of the Laitone criterion, based on rectilinear flow through a normal shock. The leading-edge coefficients exhibit more negative values, but recent laser velocimeter measurements indicate local Mach numbers close to the Laitone value.

In order to estimate the onset of the limit Mach number at the leading edge, i.e., the boundary between zones 2 and 3, equations involving the local surface curvature are used.

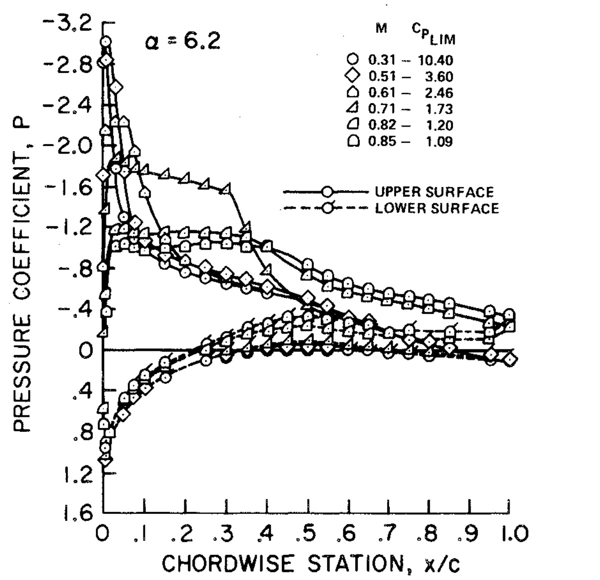

Fig. 3 Pressure distribution for the NACA 64A010 airfoil at $\alpha = 6.2°$.[6]

Equation (10) expresses the maximum local velocity ratio for potential flow around a parabolic leading edge[11]

$$\left(\frac{V_e}{V_\infty}\right)_{\max} = \sqrt{1 + \left(1 + \sqrt{\frac{r/c}{2}}\right)^2 \left(\frac{2\alpha^2}{r/c}\right)} \tag{10}$$

Equation (11) is the general isentropic relationship between local velocity and local Mach number.

$$\left(\frac{V_e}{V}\right) = \frac{M_e\sqrt{1+[(\gamma-1)/2]M^2}}{M\sqrt{1+[(\gamma-1)/2]M_e^2}} \tag{11}$$

Set

$$M_e = \sqrt{(\gamma+3)/2}$$

the Laitone limit Mach number, to obtain

$$(V_e/V)_{\max} = 1.236\sqrt{0.2 + (1/M^2)} \tag{12}$$

Equating Eqs. (10) and (12) leads to Eq. (13) for α_e.

$$\alpha_e = \frac{\sqrt{1.528 - 0.695\,M^2}}{M[1+\sqrt{2/(r/c)}]} \tag{13}$$

The onset of the limit Mach number on the leading edge implies the occurrence of "semichoked" local flow and no further increase in leading-edge thrust with further increase in angle of attack above α_e. The lift in zone 3 is evaluated in Eq. (14) as the sum of the potential lift at α_e and the additional increment of nonpotential lift for the angle increment above α_e.

$$C_L = (C_L)_{\alpha_e} + (\Delta C_L)_{\alpha - \alpha_e} \tag{14}$$

The general shape of nonpotential lift curves are compared to potential theory in Fig. 5. The high values of section lift

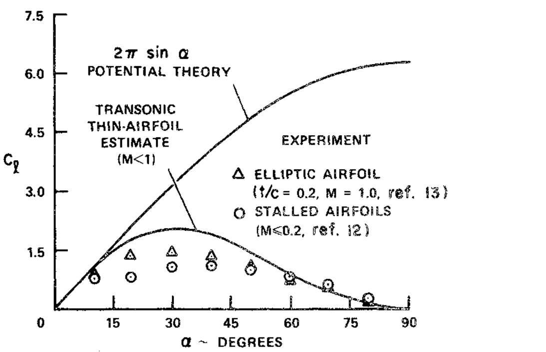

Fig. 5 Nonlinear two-dimensional lift curves.

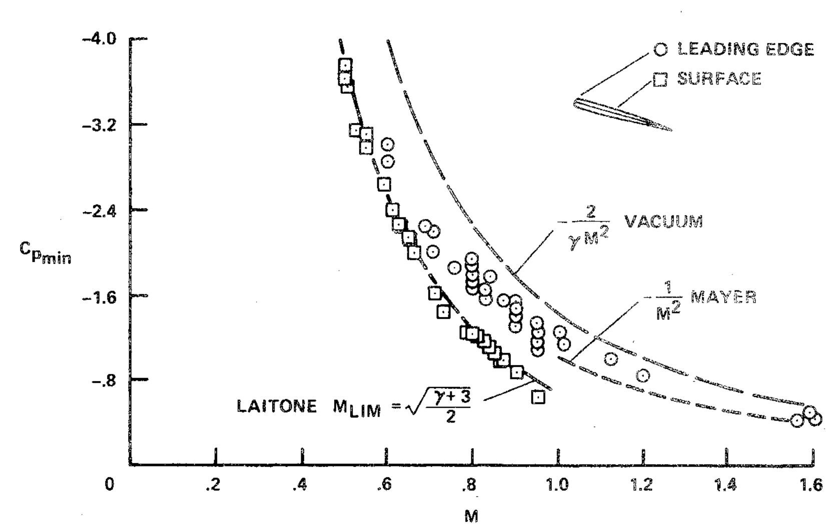

Fig. 4 Minimum pressure coefficients in transonic flow.

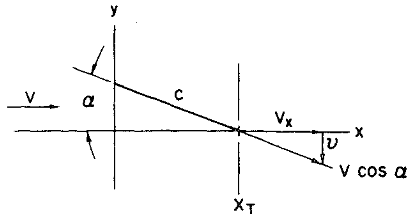

Fig. 6 Downwash momentum integral for nonpotential model.

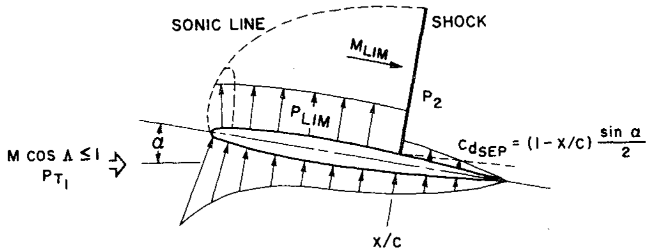

Fig. 7 Surface Mach-number-limited transonic flow.

coefficient indicated by the Kutta-Joukowski potential equation are not realized in real flows at high angles of attack, because of the occurrence of viscous stall at low speeds, typified by the circular data points,[12] or because of the onset of local Mach-limited flows at transonic speeds, typified by the triangular data points.[13] The intermediate curve represents a generalized, nonpotential lift curve that might be expected to correlate transonic thin-airfoil data characterized by the onset of the leading-edge Mach limit, the loss of leading-edge suction, or the development of flat-plate loading. A representative nonpotential lift equation (shown graphically in Fig. 6) is derived in Eqs. (15-20) from an integration of the downwash momentum in the vertical plane through the trailing edge.

$$V_x = V\left[1 - \frac{\sin^2\alpha}{1+(y/x_T)^2}\right] \tag{15}$$

$$v = V\left[\frac{\sin\alpha\,\cos\alpha}{1+(y/x_T)^2}\right] \tag{16}$$

$$d_\ell = \rho V_x v\,dy$$

$$\ell = \rho V^2 \sin\alpha\,\cos\alpha\, x_T^2 \left[\int_{-\infty}^{\infty} \frac{dy}{x_T^2+y^2} - x_T^2 \sin^2\alpha \int_{-\infty}^{\infty} \frac{dy}{(x_T^2+y^2)^2}\right] \tag{17}$$

$$c_\ell = 2\pi \sin\alpha\,\cos^2\alpha[1-(\sin^2\alpha)/2] \tag{18}$$

$$dc_\ell/d\alpha = \pi\cos\alpha(2\sin^4\alpha + 2\cos^2\alpha - 4\sin^2\alpha - 3\sin^2\alpha\cos^2\alpha) \tag{19}$$

$$c_{d_i} = c_\ell \tan\alpha \tag{20}$$

Two simplifying assumptions are made in the analytical model. First, the nondimensionalized downwash attenuation factor $(1/(1+y^2/x_T^2)$ from potential flow is used in the momentum integration. Second, the velocity leaving the trailing edge is set equal to $V\cos\alpha$. This is the simplest velocity vector that satisfies the boundary conditions of zero lift at 0° and 90° angles of attack and provides for stream velocity V at the trailing edge at 0°. It also implies trailing-edge pressure coefficients in the range of 0 to 0.2 typified in experiments (Fig. 3) prior to the onset of marked separation.

The nonpotential lift increments are adjusted by the same aspect-ratio and lower-surface compressibility factors as applied to potential lift increments. The maximum value of the nonpotential lift, computed from Eq. (18), occurs at 31° angle of attack.

D. Surface Mach-Limited Aerodynamics (Zone 4)

The conceptual flow model depicting surface Mach-number-limited flow is shown in Fig. 7 and Eqs. (21-25)

$$c_{d_{sep}} = (1-x/c)(\sin\alpha)/2 \tag{21}$$

$$\frac{d(P_2/P_{T_1})}{dM_{loc}} \equiv 0 \qquad M_{\lim} = \sqrt{\frac{\gamma+3}{2}} \tag{22}$$

$$C_{P_{\lim}} = \frac{2}{\gamma M^2}\left\{\frac{\{1+[(\gamma-1)/2]M^2\cos^2\bar{\Lambda}_{xc}\}^{\gamma/(\gamma-1)}}{3.58} - 1\right\} \tag{23}$$

$$C_L = -\left[C_{P_{\lim}}\left(\frac{x}{c}\right) + \frac{1}{2}C_{P_2}\left(1-\frac{x}{c}\right)\right]\cos\alpha + \bar{F}_\ell C_{L_\ell} \tag{24}$$

$$C_{D_i} = (C_L{}^2/\pi A) + C_L(\tan\alpha)^d + C_{D_{sep}} \tag{25}$$

The component of Mach number normal to the leading edge is less than or equal to unity. Laitone[4] used the maxima of the derivative of the pressure ratio with respect to the local Mach number ahead of the shock to define the limit Mach number, Eq. (22). The limit pressure coefficient given in Eq. (23) accounts for sweep or obliqueness of the shock and reduces to Laitone's pressure coefficient for zero sweep.

The lift on the upper surface is evaluated in Eq. (24) as the limit pressure coefficient multiplied by the fraction of the chord ahead of the shock plus the pressure coefficient behind the shock linearly attenuated to zero at the trailing edge and multiplied by the remaining fraction of the chord. Flow separation at the shock is assumed to take place when the limit surface Mach number is reached. The separation drag coefficient given by Eq. (21) accounts for the momentum decrement in the separated wake. The wake is modeled to have a linear velocity profile whose upper edge follows a line from the base of the shock at an inclination of half of the angle of attack.

The lower-surface lift coefficient of Eq. (24) is the compressible, nonpotential value. To provide mathematical smoothness and agreement with experiments throughout transonic Mach numbers, tan α in Eq. (25) is varied exponentially with Mach number. Note that, although the limit Mach number is constant, the lift and induced drag coefiicients in zone 4 vary with α and with M, including the dependency on $C_{P_{\lim}}$ and $\bar{F}_\ell$.

E. Supersonic Flow (Zone 5)

As the component of freestream Mach number normal to the leading edge traverses unity, the shock on the upper surface moves to the trailing edge, and bow shocks appear at the leading edge. For the majority of cases, blunt airfoils are used, and the bow shocks are detached. The following empirical equations [Eqs. (26-32)] will be shown to give reasonable agreement with experiment for Mach numbers up to 2.0. They are based on the nonpotential equations derived earlier with an aspect-ratio factor approaching unity at high supersonic Mach numbers.

$$C_L = C_{L_u} + C_{L_\ell} \tag{26}$$

$$C_{L_u} = \text{lesser of} \begin{cases} -C_{P_{\lim}}\cos\alpha \\ \left(\dfrac{A}{A+2/M}\right)\dfrac{c_\ell}{2M^{2/3}}(GU) \end{cases} \tag{27}$$

$$C_{P_{\lim}} = -\frac{1}{M^2}\left(1-\frac{0.32}{M^{2.5}}\right) \tag{28}$$

$$c_\ell = 2\pi\sin\alpha\cos^2\alpha\left(1-\frac{\sin^2\alpha}{2}\right) \tag{29}$$

$$C_{L_\ell} = \frac{C_{P_{\mathrm{stag}}}}{M^{2/3}}\left(\frac{A}{A+2/M}\right)\frac{c_\ell}{2}(GL) \tag{30}$$

$$\frac{\mathrm{d}C_L}{\mathrm{d}\alpha} = \frac{C_{P_{\mathrm{stag}}}}{M^{2/3}}\left(\frac{A}{A+2/M}\right)\frac{(\mathrm{d}c_\ell/\mathrm{d}\alpha)}{2}(GL)$$

$$+\text{lesser of}\begin{cases} C_{P_{\mathrm{lim}}}\sin\alpha \\ \dfrac{A}{A+2/M}\dfrac{(\mathrm{d}c_\ell/\mathrm{d}\alpha)}{2M^{2/3}}(GU)\end{cases} \tag{31}$$

$$C_{D_i} = C_L\tan\alpha \tag{32}$$

Here $GU = 1 = (M-0.2)^{-1}$ if $M>1.2$; $GL = 0.7 = 1.6-0.6M$ if $M \leq 1.5$.

A transition is made in the upper-surface limit pressure coefficient of Laitone to the empirical value suggested by Mayer.[14] The proportion of the total lift contributed by the upper surface decreases with increasing supersonic Mach number and minimizes the importance of the supersonic limit pressure coefficient. A summary of the equations for the lift and induced drag coefficients for the wings in each of the flow regimes is presented in Table 1.

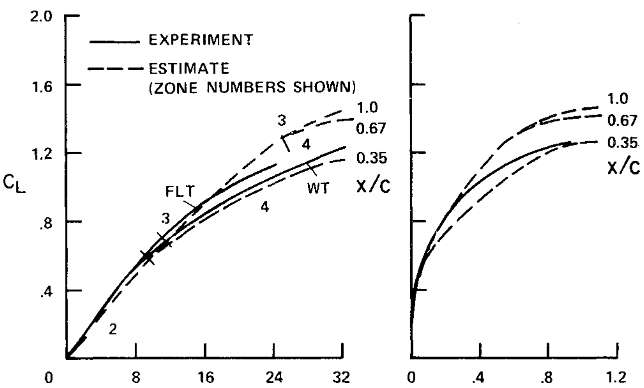

Fig. 8 Lift and induced drag for the F4C at $M = 0.9$.

III. Application to Complete Aircraft Configurations

The foregoing discussion dealt with the estimation of the lift on the wing to high angles of attack. In order to estimate complete aircraft aerodynamics, the force contributions of the other components are evaluated. In the present calculations, no account is made for forces on inlets, nacelles, or afterbodies. The afterbody is assumed to be aligned closely with the flow leaving the wing trailing edge (undeflected flap).

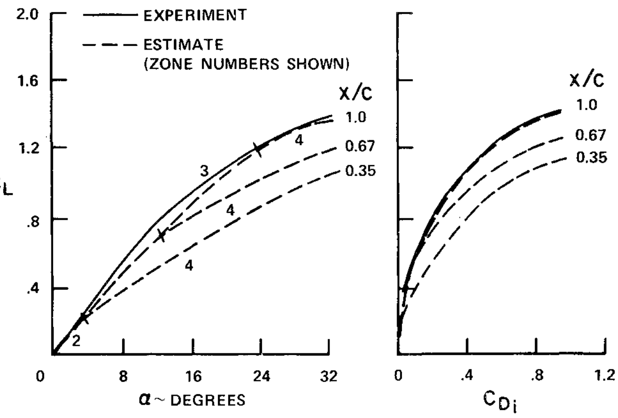

Fig. 9 Lift and induced drag for the F4C at $M = 1.2$.

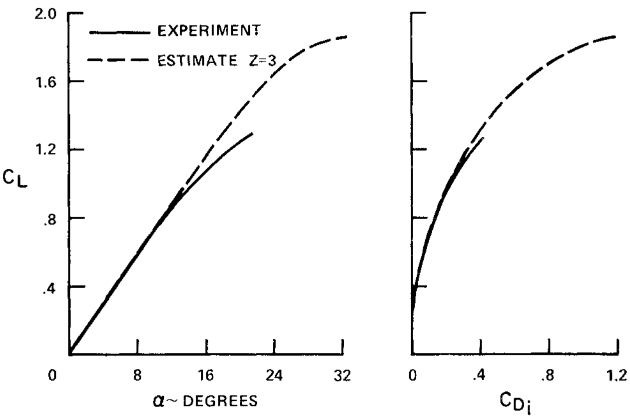

Fig. 10 Lift and induced drag for the F-5A at $M = 0.8$.

Table 1 Summary of aerodynamics and flow regimes

Zone	Dominant feature	Three-dimensional lift and induced drag coefficients for wings
1	Viscous separation	Not covered
Boundary 1-2		Not covered
2	Compressible shock-free	$C_L = 2\pi\sin\alpha[A/(A+2)]\cos\bar{\Lambda}[(\bar{F}_u+\bar{F}_\ell)/2]$ $C_{D_i} = C_L{}^2/\pi A$
Boundary 2-3	See Eq. (13) for α_e	
3	Leading-edge Mach-number	$C_L = \text{greater of}\begin{cases}\text{transitional } C_L = (C_{L_{Z=2}})_{\alpha_e} + \tfrac{1}{2}(\mathrm{d}C_L/\mathrm{d}\alpha)_{Z=3}(\alpha-\alpha_e)(1+\bar{F}_\ell) \\ \text{nonpotential } C_L = \pi\sin\alpha\cos^2\alpha[1-(\sin^2\alpha/2)][A/(A+2)]\cos\bar{\Lambda}(1+\bar{F}_\ell)\end{cases}$ $C_{D_i} = (C_L{}^2/\pi A) + C_L(\tan\alpha)^{\mathrm{d}}$
Boundary 2-4 or 3-4	$C_{L_{Z=2,3}} = C_{L_{Z=4}}$	
4	Surface Mach-number	$C_L = [C_{P_{\mathrm{lim}}}(x/c) + \tfrac{1}{2}C_{P_2}(1-x/c)]\cos\alpha + \bar{F}_\ell\pi\sin\alpha\cos^2\alpha(1-\sin^2\alpha/2)(A/(A+2)\cos\bar{\Lambda}$ $C_{D_i} = (C_L{}^2/\pi A) + C_L(\tan\alpha)^{\mathrm{d}} + C_{D_{\mathrm{sep}}}$
Boundary 4-5	$M\cos\bar{\Lambda}_{\mathrm{l.e.}} = 1$	
5	Supersonic	$C_{L_u} = \text{lesser of}\begin{cases}(1/M^2)[1-(0.32/M^{2.5})]\cos\alpha \\ (c_\ell/2M^{2/3})[A/(A+2/M)](GU)\end{cases}$ $C_{l_\ell} = c_\ell/2[A/(A+2/M)](C_{P_{\mathrm{stag}}}/M^{2/3})(GL)$ $C_{D_i} = C_L\tan\alpha$ $C_L = C_{L_u} + C_{L_\ell}$ $c_\ell = 2\pi\sin\alpha\cos^2\alpha[1-(\sin^2\alpha)/2]$

The force on the nose is estimated by the method summing the slender-body contribution and the viscous crossflow drag, an updated discussion of which is presented in Ref. 15.

Equations (33-36) were determined from an empirical correlation of the available downwash information presented in Refs. 16-19.

wake angle

$$\epsilon_W = \frac{\alpha(3.9-A^{3-A})}{3\sqrt{1+TR}}\left[\frac{2}{A}+0.1\left(\sqrt{\frac{b/2}{3\bar{c}/4}}+\sqrt{\frac{b/2}{\ell_T}}\right)\right] \tag{33}$$

tail offset from wake

$$\left|\frac{y}{b/2}\right| = \left|\frac{y_0}{b/2}+\left(\frac{\ell_t}{b/2}-\frac{1.5}{A}\right)\sin\epsilon_W-\frac{\ell_t}{b/2}\sin\alpha\right| \tag{34}$$

downwash angle at tail

$$\epsilon = \frac{\alpha(3.9-A^{3-A})}{3\sqrt{1+TR}}\left[0.2\sqrt{\frac{b/2}{\ell_t}}+\frac{2}{A}\right]\left[\frac{2}{3}+\frac{1}{3}\cos\left(\frac{9}{4}\alpha\right)\right]\left[1-\frac{3}{2}\left|\frac{y}{b/2}\right|\right] \tag{35}$$

downwash derivative

$$\frac{d\epsilon}{d\alpha} = \frac{(3.9-A^{3-A})}{9\sqrt{1.TR}}\left[0.2\sqrt{\frac{b/2}{\ell_t}}+\frac{2}{A}\right] \times \left[2+\cos\left(\frac{9}{4}\alpha\right)-\frac{9}{4}\alpha\sin\left(\frac{9}{4}\alpha\right)\right]\left[1-\frac{3}{2}\left|\frac{y}{b/2}\right|\right] \tag{36}$$

The aerodynamic characteristics of the horizontal tail are determined in the same manner as used for the wing, taking into account areas, aspect ratios, and angles of attack. Longitudinal moment and trim characteristics also are calculated using the present nonlinear aerodynamics.

The method has been programmed and consists of approximately 400 cards for the wing aerodynamics, 200 for the tail and trim characteristics, and 40 for the nose. Calculations for six Mach numbers and 20 angles of attack require 1 sec on the IBM 360 and 0.05 sec on the CDC 7600, with a 3.3-k bit memory.

IV. Comparisons of Experiment and Estimate

Several comparisons of experimental data and estimates are presented in Figs. 8-14. The characteristics for the F-4 were taken from Ref. 20, for the F-5 from Refs. 21 and 22, and for a conceptual fighter model from Ref. 23. (The wing leading-edge sweep angles for the three cases are 51.4°, 31.9°, and 50.0°, respectively.)

For expediency, the estimates are based on assumed average values applied across the wing span rather than on parameters with designated variations across the span. For example, calculations are based on the average leading-edge radius and the designated chordwise shock locations are assumed to be the same for all wing span stations. Many refinements can be incorporated into the method, but its usefulness can be demonstrated by the present simplified estimates.

The comparison in Fig. 8 indicates that the agreement between experiment and estimate would be improved for a shock location near midchord. One might be able to deduce this from flow visualizations, pressure distributions, or from inspection of the longitudinal area distribution relative to the chordwise locations of the mean aerodynamic chord. The

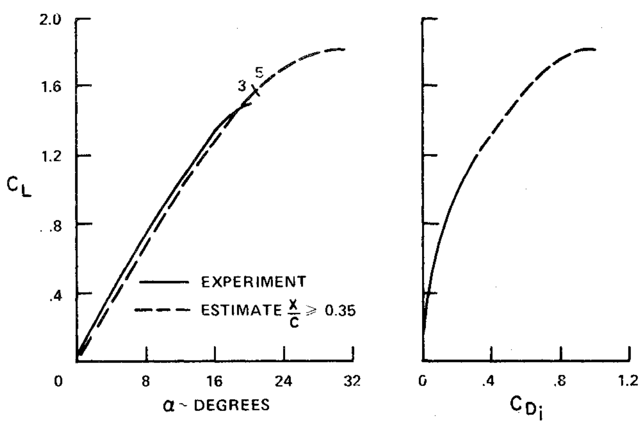

Fig. 11 Lift and induced drag for the F-5A at $M = 1.15$.

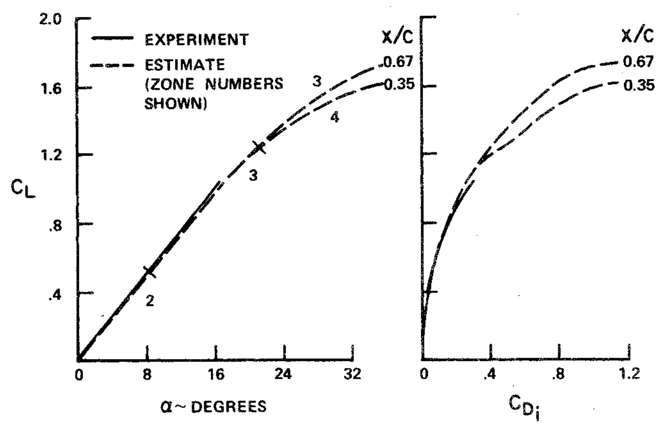

Fig. 13 Lift and induced drag for model L at $M = 0.8$.

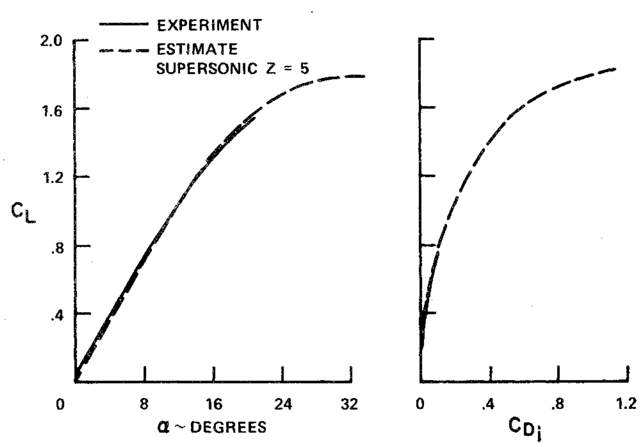

Fig. 12 Lift and induced drag for the F-5A at $M = 1.25$.

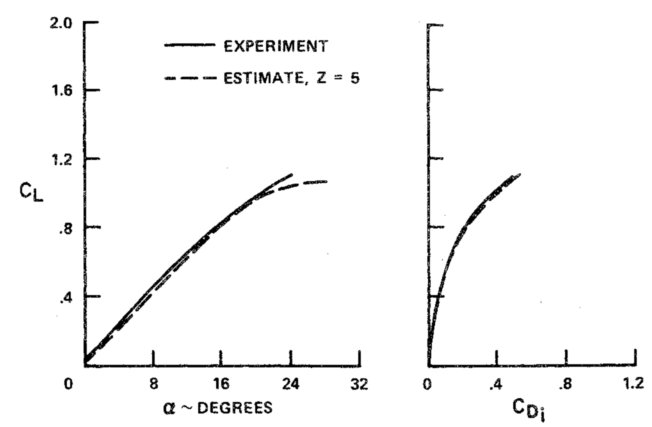

Fig. 14 Lift and induced drag for model L at $M = 1.8$.

reduction in lift-curve slope accompanying onset of the surface Mach number limit (zone 4) is apparent in the estimates. The results in Fig. 9 indicate that the shock is well rearward on the wing, at least on the inboard portion, or additional lift is being gained from aircraft components not covered in the present method.

The estimate in Fig. 10 remains in zone 3 throughout the range of angles of attack. The falling off of the experimental lift and the increased drag possibly might be attributed to separation unaccounted for in the present method. The results shown in Figs. 11 and 12 indicate excellent agreement between estimate and experiment, even though the latter has a small camber lift coefficient at zero angle of attack.

The results shown in Figs. 13 and 14 indicate good agreement for the limited range of angles of attack covered in the experiment. Configurations testing above 20° is needed for additional models in order to correlate these and other analytical approaches for estimating aerodynamics to high angles of attack.

V. Concluding Remarks

An analytical method has been formulated for estimating lift and induced drag to high angles of attack, with emphasis on transonic speeds. The method is well suited to computerized preliminary design and optimization studies. New features in the method include separate compressibility factors for the upper and lower wing surfaces; applications of Latione's limit Mach-number criterion to the curvilinear flow around the leading edge and to the rectilinear flow along the airfoil upper surface to the shock wave; and the use of a nonpotential lift equation derived from the integration of downwash momentum in the transonic-flow approximations. The method accounts for nose lift, for the wing downwash field and tail lift, and for longitudinal trim and demonstrates reasonable agreement with experiment.

Acknowledgment

This work was performed at NASA Ames Research Center.

References

[1]Nelms, W. P. and Axelson, J. A., "Preliminary Performance Estimates of a Highly Maneuverable Remotely Piloted Vehicle," NASA TN D-7551, Feb. 1974.

[2]Smith, A. M. O., "High-Lift Aerodynamics," 1974 Wright Brothers Lecture, *Journal of Aircraft*, Vol. 12, June 1975, pp. 501-530.

[3]Chapman, D. R., Mark, H., and Pirtle, M. W., "Computers vs. Wind Tunnels for Aerodynamic Flow Simulations," *Astronautics & Astronautics*, Vol. 13, April 1975, pp. 22-30.

[4]Laitone, E. V., "Limiting Velocity by Momentum Relations for Hydrofoils Near the Surface and Airfoils in Near Sonic Flow," *Proceedings of the Second U.S. National Congress of Applied Mechanics*, June 14-18, 1954, pp. 751-753.

[5]Liepmann, H. W. and Roshko, A., *Elements of Gas Dynamics*, Wiley, New York, 1957, Chap. 10.

[6]Stivers, L. S., Jr., "Effects of Subsonic Mach Number on the Forces and Pressure Distributions on Four NACA 64A-Series Airfoil Sections at Angles of Attack as High as 28°," NACA TN 3162, March 1954.

[7]Chaplygin, S., "Gas Jets," NACA TM 1063, 1944.

[8]Axelson, J. A. and Stevens, G. L., "Investigation of a Slat in Several Different Positions on an NACA 64A010 Airfoil for a Wide Range of Subsonic Mach Numbers," NACA TN 3129, March 1954.

[9]Cahill, J. F. and Cooper, B. L., "Flight Test Investigation of Transonic Shock-Boundary Layer Phenomena," Air Force Flight Dynamics Lab., AFFDL-TR-68-84, July 1968.

[10]Pearson, E. O., Jr., "Effect of Compressibility on the Distribution of Pressures over a Tapered Wing of NACA 230-Series Airfoil Sections," NACA TN 1390, July 1947.

[11]Ericsson, L. E. and Reding, J. P., "Stall-Flutter Analysis," *Journal of Aircraft*, Vol. 10, Jan. 1973, pp. 5-13.

[12]Wick, B. H., "Study of the Subsonic Forces and Moments on an Inclined Plate of Infinite Span," NACA TN 3221, June 1954.

[13]Randall, G. A., "Aerodynamic Characteristics of Two 20 Percent Thick, Rectangular Wings Up to 90° Angle of Attack at Subsonic, Transonic, and Supersonic Speeds," Aerostructures, Inc., NASA Contract NAS 2-3814, April 1967.

[14]Mayer, J. P., "A Limit Pressure and an Estimation of Limit Forces on Airfoils at Supersonic Speeds," NACA RM L8F23, 1948.

[15]Jorgensen, L. H., "Prediction of Static Aerodynamic Characteristics for Space Shuttle-Like and Other Bodies at Angles of Attack from 0° to 180°," NASA TN D-6996, 1973.

[16]Perkins, C. D. and Hage, R. E., *Airplane Performance, Stability and Control*, Wiley, New York, 1949.

[17]Silverstein, A. and Katzoff, S., "Design Charts for Predicting Downwash Angles and Wake Characteristics Behind Plain and Flapped Wings," NACA TR 648, 1939.

[18]Axelson, J. A., "Downwash Behind a Triangular Wing of Aspect Ratio 3—Transonic Bump Method," NACA RM A53123, 1956.

[19]Decker, J. L., "Predictions of Downwash at Various Angles of Attack for Arbitrary Tail Locations," *Aeronautical Engineering Review*, Vol. 15, Aug. 1956, pp. 22-27.

[20]Woods, A. R., "Performance Data and Substantiation," McDonnell Aircraft Co., Dec. 1973.

[21]Ackerman, N. G. and Warren, B. L., "F-5 Basic Aerodynamic Drag Data," Northrop Corp., Norair Rept. NOR 64-2, Jan. 1964.

[22]Levin, A. D. and Petroff, D. N., "An Experimental Investigation of Single and Double-Hinged Leading-Edge Flaps on a Model of an F-5A Aircraft at Transonic Mach Numbers," NASA TM X-62,095, Jan. 1972.

[23]Dollyhigh, S. M., "Subsonic and Supersonic Stability and Control Characteristics of an Aft Tail Fighter Configuration with Cambered and Uncambered Wings and Uncambered Fuselage," NASA TM X-3078, 1974.